OPEN

Graphene/Si-nanowire heterostructure molecular sensors

Jungkil Kim, Si Duk Oh, Ju Hwan Kim, Dong Hee Shin, Sung Kim & Suk-Ho Choi

Department of Applied Physics, College of Applied Science, Kyung Hee University, Yongin 446-701, Korea.

Wafer-scale graphene/Si-nanowire (Si-NW) array heterostructures for molecular sensing have been fabricated by vertically contacting single-layer graphene with high-density Si NWs. Graphene is grown in large scale by chemical vapour deposition and Si NWs are vertically aligned by metal-assisted chemical etching of Si wafer. Graphene plays a key role in preventing tips of vertical Si NWs from being bundled, thereby making Si NWs stand on Si wafer separately from each other under graphene, a critical structural feature for the uniform Schottky-type junction between Si NWs and graphene. The molecular sensors respond very sensitively to gas molecules by showing 37 and 1280% resistance changes within 3.5/0.15 and 12/0.15 s response/recovery times under O_2 and H_2 exposures in air, respectively, highest performances ever reported. These results together with the sensor responses in vacuum are discussed based on the surface-transfer doping mechanism.

R ecently, semiconductor nanowires (NWs) have received much attention due to their crucial role in the physicochemical science and their high potential for practical applications in advanced devices such as transistors, light-emitting-diodes, solar cells, bio/chemical sensors, and etc[1–7]. Especially, vertically-aligned Si NWs have been considered as a strong candidate for building blocks of advanced devices because of their high aspect ratio and high volume/surface ratio originating from the vertical structure[8–13]. For the applications of vertical Si NWs in practical devices such as sensors[14], it is important to make a continuous electrode on the tips of Si NWs for uniform electrical contact between the electrode and Si NWs. In the previous studies for forming the top electrode, tips of NWs were covered with polymer (or other insulators), subsequently opened partially by O_2 plasma or other etching methods, and finally the metal film was deposited on the opened tips of NWs[15–17]. However, these methods limit the use of NWs in enhancing the device performances due to several reasons. As one reason, the polymer (or other insulators) covering the upper part of the tips causes an efficiency drop because the polymer (or other insulators) makes a dent in the region exposed to atmosphere. Also, it requires complicated processes to cover the polymer on the tips of Si NWs and open the tip part partially. Moreover, since the polymer acts as a barrier layer between the Si NWs and the electrode, it can increase the operation voltage and produce many heat-related problems, thereby decreasing the product durability. In case of Si-NW sensors, the contact between polymer and Si NWs can induce a high dark current and a low on/off ratio, which makes it difficult to detect the fine change caused by small stimulus[14].

In our previous work, we reported the electrical behaviors of the contact between undefined graphene and irregular-shaped and randomly-arranged Si NWs with very sharp tips, resulting in non-uniform contact of the electrode with NWs, thereby giving rise to low-quality device performances[18]. Here, for overcoming the drawbacks of the polymer (or other insulators)-based Si-NW devices, we employ graphene as a barrier layer for forming an electrical junction between high-density vertically-aligned Si-NW arrays and graphene because graphene has outstanding properties such as high carrier mobility, extremely-strong mechanical strength, and chemical stability[19–24]. We also show that the graphene/Si-NW heterostructures exhibit Schottky-diode behaviors and act well as a molecular sensor under H_2 and O_2 exposures.

Results

Fabrication and structural characterization. As schematically shown in Fig. 1a and b, single-layer graphene was transferred onto the top of vertically-aligned Si NWs, and subsequently dried on a hot plate firstly at 80°C for 3 h and secondly at 130°C for 3 h to fabricate the graphene/Si-NW heterostructures. Fig. 1e shows an optical image of a graphene/Si-NW heterostructure whose lateral area is more than 3×3 cm². As shown in a scanning electron microscope (SEM) image of Fig. 2a, one portion of Si NWs is covered with graphene, thereby forming a boundary interface between graphene and NWs, and the other portion of Si NWs is opened without graphene. A cross-
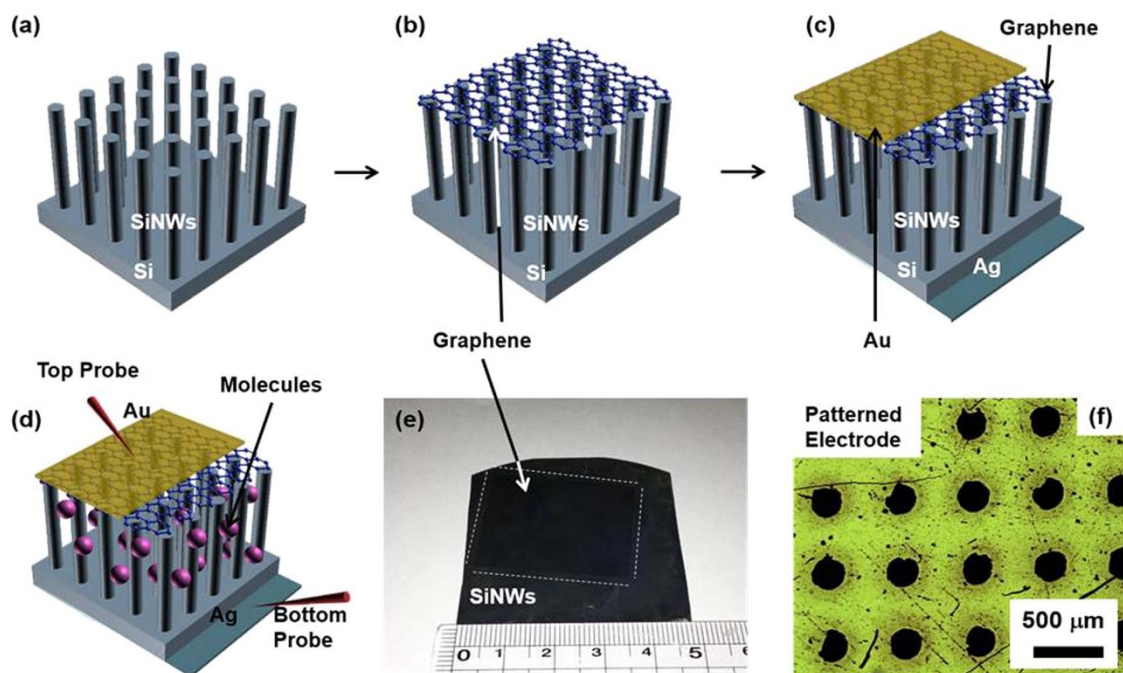
Figure 1 | Schematics and images describing device fabrication processes. (a), (b), and (c) Schematic illustrations of the processes to fabricate graphene/Si-NW array heterostructure molecular sensor. (d) Measurement configuration for characterizing the molecular sensor. (e) Optical microscopic image of graphene/Si-NW heterostructure over large area. (f) Optical microscopic image of a top Au electrode patterned into 200 μm-size hole arrays.

sectional SEM image in Fig. 2b shows the tips of Si NWs very uniformly attached with graphene layer, thereby leading to fine electrical contact between Si NWs and graphene. Since large-scale graphene can act as a spreading semi-metallic layer for forming uniform junction with the tips of Si NWs, direct deposition of a metal film on graphene completes the graphene/Si-NW device structure.

In the whole procedures to fabricate graphene/Si-NW structures, it is important for well-aligned vertical Si NWs to be employed as a building block. If unordered Si NWs are utilized as reported before[18], the Si NWs are assembled into bundles seriously due to their irregular length, diameter, position, and shape. As a result, graphene is harshly damaged, as shown in a high-magnification SEM image (Supplementary Fig. S1a). When graphene is transferred on the top of well-aligned Si NWs, it will hold the tips of Si NWs, thereby preventing them from being bundled under graphene to a certain degree, even though tips of Si NWs are not perfectly separated. While Si NWs are preserved in DI water after the native oxide of Si NWs is
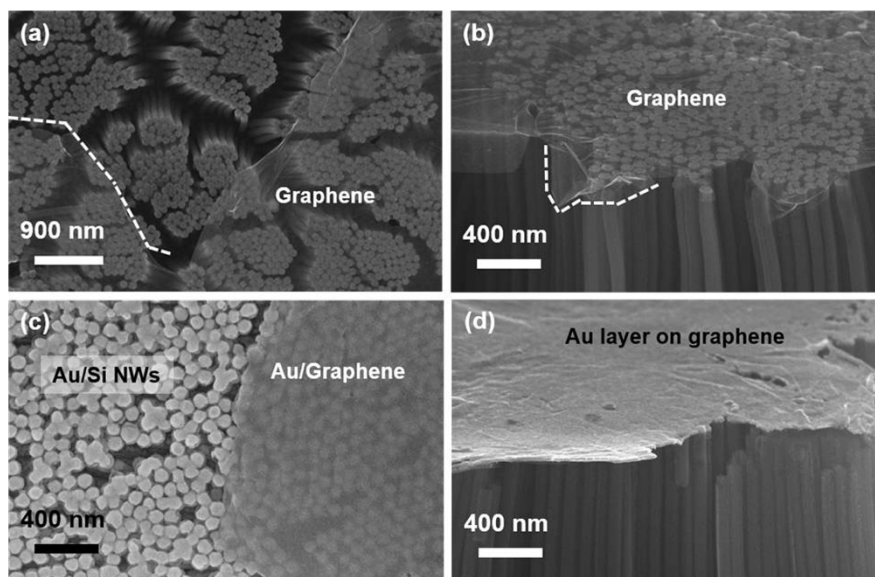

Figure 2 | SEM images of graphene/Si-NW heterostructures. (a) Plan-view image of the graphene/Si-NW heterostructure. The dark blanket on tips of Si NWs is the graphene sheet. (b) Tilted-view image of graphene/Si NWs confirming the uniform contact between graphene and Si NWs. A small piece of graphene is sagged to the side of Si NWs, which may be formed when the sample was cut for the SEM investigation. (c) Plan-view image of an Au film on graphene and tips of Si NWs. A continuous Au film is formed only on graphene. (d) Tilted-view image of Au/graphene/Si NWs. A continuous Au film is well placed on the graphene/Si NWs.
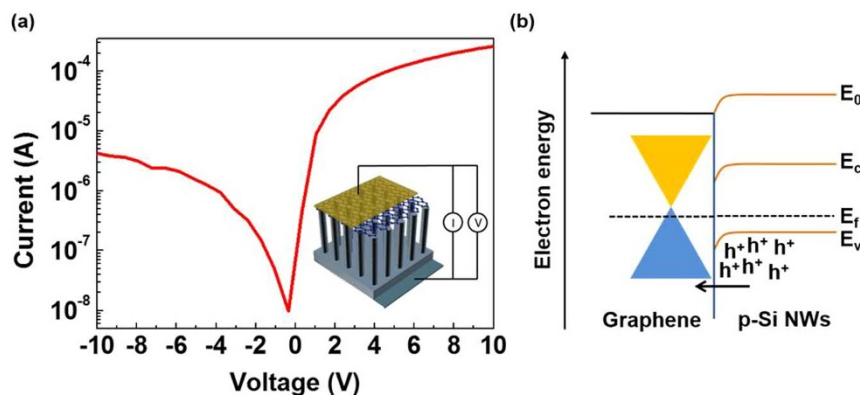
Figure 3 | I-V characteristics and band diagrams. (a) *I-V* curve of graphene/Si-NW array heterostructure, together with a schematic illustration of the measurement configuration. (b) Energy band diagram of graphene/Si-NW heterostructure.

etched for the good contact with the graphene, the surfaces of the NWs are at liquid/solid phase. If the Si NWs are taken out and dried in air, the surfaces of the Si NWs are partially at liquid/solid or gas/solid state, resulting in surface tension[14], thereby making the tips of the NWs bundled. Therefore, the Si NWs were not dried until the graphene-transfer process started. After the graphene was transferred onto tips of Si NWs, it was dried on a hot plate firstly at 80°C for 3 h and secondly at 130°C for 3 h for achieving good contact of graphene onto tips of Si NWs. As shown in a SEM image of Fig. 2b, the graphene-transferred Si NWs stand vertically and separately to a certain extent. Separation of tips is a critical structural feature for the uniform electrical contact between Si NWs and the graphene.

A 15-nm-thick Au thin film as a top electrode was deposited on graphene by e-beam evaporation, as shown in Fig. 1c. Fig. 2c shows a SEM image of the Au film uniformly formed on graphene, in strong contrast with the case of unordered Si NWs (Supplementary Fig. S1b), as reported before[18]. The Au film is uniformly connected with whole tips of Si NWs, as confirmed in a cross-section SEM image of Fig. 2d. The Au film as well as the graphene is uniformly formed over extended area of Si-NW tips, as shown by the SEM images (Supplementary Fig. S2). On the other hand, Au lumps and nanoparticles (NPs) are formed on an opened part of tips and sides of Si NWs (Supplementary Fig. S3). For the application of the graphene/Si NWs structures to molecular sensors, the gas molecules for the detection test should have easy access to the surface of Si NWs. For this, the top electrode was patterned with arrays of 200 μm-sized holes by reactive ion etching (RIE) process using Ar gas through the stainless shadow mask, as shown in Fig. 1f.

I-V characteristics. Fig 3a shows typical dark *I–V* characteristics of the graphene/Si-NW heterojunction device, with an inset illustration that describes the measurement configuration. Silver paste was used to form the top and bottom contacts on the Au film and the Si wafer, respectively. Forward bias is defined as negative voltage applied to the graphene layer. The heterojunction device is highly rectifying with an 'on/off' current ratio of ~10^2 at ±5 V, indicating well-defined behaviors of Schottky diodes. The nonlinear *J-V* characteristics of the Schottky junction can be expressed by the thermionic emission model[25]

$$J = J_s \left[\exp\left(\frac{-qV}{nkT} \right) - 1 \right] \quad (1)$$

where J_s is the reversed saturated current density and *n* is the diode ideality factor, which can be estimated to be ~ 1.93, from the slope of the dark *I-V* curve derived through curve fitting, smaller than those previously reported for the graphene/Si-NW heterojunctions[26,27].

The *I-V* behaviors can be explained based on the energy band diagram, as shown in Fig. 3b. Due to the formation of the Schottky barrier at the graphene/Si NW interface, partial carriers in Si NWs tend to move to the graphene side and consequently, the energy levels near the Si NW surface will bend downward (Si NW is p-type), causing the formation of space-charge region and built-in electric field near the graphene/Si NW interface. Under reverse bias, majority carrier holes have to overcome the enhanced barrier between graphene and Si NWs to move from Si NWs to graphene, thereby inducing negligible current in the negative bias, as shown in Fig. 3a. In contrast, under forward bias, holes move easily to graphene from Si NWs over the lowered barrier, resulting in high magnitude of current in the positive bias, as shown in Fig. 3a.

Molecular sensing characteristics. Fig 4 shows electrical responses of the graphene/Si-NW diode as a molecular sensor to periodic
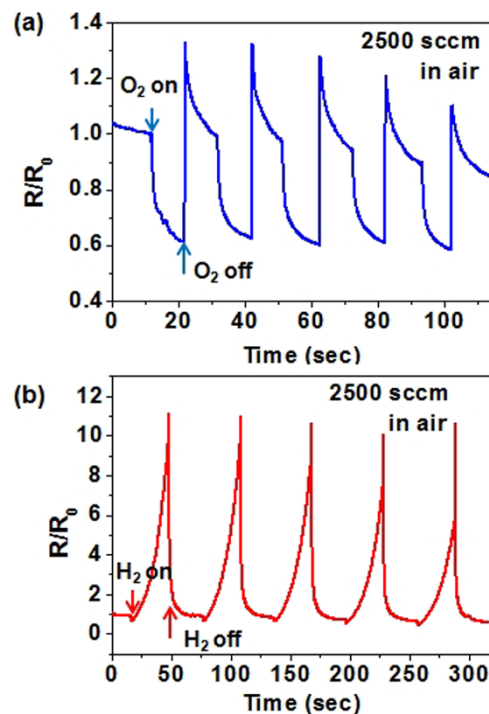

Figure 4 | Responses to gas exposures. Normalized resistance responses of graphene/Si-NW heterostructure molecular sensor under repeated exposures of (a) O_2 and (b) H_2 gases in air at room temperature. Exposure intervals of O_2 and H_2 gases are 10 and 30 s, respectively.

switches of 99.999% O_2 and H_2 exposures with intervals of 10 and 30 s at a flow rate of 2500 sccm, respectively in air at room temperature. During these time intervals the resistance reaches almost its saturation value for each gas. A forward bias of 3 V was applied during the molecular sensing. The sensor responded very sensitively and periodically to the cyclically-changing exposures of each gas. The resistance of the sensor is estimated to decrease by 37% upon the release of oxygen gas molecules. In contrast, the resistance increases by 1280% by exposure to hydrogen gas molecules. For lower flow rates of 200/500/1500 sccm, the resistance changes were reduced to 17/23/28 and 340/370/490% under O_2 and H_2 exposures, respectively (Supplementary Fig. S4).

The observed sensor response can be explained based on the surface-transfer doping effect[28,29]. Electrons in p-type Si NWs are trapped by oxygen molecules that are adsorbed on surface of Si NWs[29,30], which could form ionized oxygen[31,32] such as O^{2-} by oxygen redox reaction $O_2 + 4e^- \rightarrow 2O^{2-}$, resulting in the injection of holes (majority carriers of p-type Si) into the valence band of Si NWs. Then, the holes accumulated in p-type Si NWs enhances the conductance (or reduces the resistance), as shown in Fig. 4(a). In contrast, hydrogen molecules adsorbed on surface of p-type Si NWs extract holes from Si NWs (i.e., surface trapping of majority carriers), which could form ionized hydrogen by the hydrogen redox reaction $H_2 + 2h^+ \rightarrow 2H^+$, resulting in the reduction of the conductance (or enhancing the resistance), as shown in Fig. 4(b). When the sensor is exposed to gas molecules, its resistance is changed instantly and reaches gradually the relatively-stable value. When the gas exposure is subsequently ceased, the resistance is recovered to its initial value very quickly. The response/recovery times, defined as the times required for the resistance to restore 30% of its total change during the on/off interval, are estimated to be about 3.5/0.15 and 12/0.15 s for oxygen and hydrogen gas molecules, respectively, much shorter than those previously reported[14,33,34]; ~ 20/20 s, ~180/30 s, and ~300 s/not available.

The characterization of the molecular sensors was also performed in vacuum condition. The resistance changes were measured under exposures of air, oxygen, and hydrogen (500 ml/min) into the vacuum chamber of 3 L volume at a working pressure of 30 mTorr after it had been evacuated down to 1 mTorr. The resistance of the sensor decreases by 6 and 2.3% upon the release of oxygen and air molecules, respectively (Supplementary Fig. S5). The responsivity of the sensor to the oxygen molecules is much lower in vacuum than in air. The hydrogen molecules gave almost no specific effects on the resistance of the sensor in vacuum. The H_2O molecules are usually attached to the Si surface as forms of molecular H_2O or dissociated H and OH[35,36] in air by bonding the H_2O, H, or OH species to the dangling bonds belonging to different atoms on the Si surface[36]. The dangling bonds can act as defects trapping the majority carriers of Si NWs, thereby reducing the conductance. In vacuum, the dangling bonds are not passivated due to negligible adsorption of H_2O or dissociated H and OH on the Si NW surface, resulting in the reduction of the sensor responsivity. The oxygen molecules are thought to be attached on the surface of Si NWs while they are preserved in air, judging from the sensor response to the air molecules in vacuum (Supplementary Fig. S5). This and passivation of dangling bonds in air would result in such strong sensor response to the hydrogen molecules in air. In contrast, the NW surface is cleaned in vacuum, resulting in negligible formation of adsorption sites for hydrogen, such as O_2^- site, in addition to negligible passivation of dangling bonds, thereby showing almost no sensor response to hydrogen molecules in vacuum.

Discussion

Despite repeated on/off tests of gas exposures, the resistance responses of the sensors were very regular and periodical. Even though several studies were presented on the sensing performance of Si NW-

based devices, to the best of our knowledge, the functionality of the graphene/Si NW heterostructure sensor in this work is extremely high, especially in the response (1280%) to the hydrogen exposure, compared to the previous report (~20%)[14]. The outstanding sensing properties of the molecular sensors might be caused by efficient utilization of the whole surface area of individual Si NWs. Such structural feature leads to the high on/off ratio, thereby enabling the sensors to detect even the fine change of the resistance caused by little exposure of the gas molecules. Conventional NW sensors are of a lateral configuration[30,37–39], thereby limiting their sensing efficiency. In addition, the graphene electrode could also play as a role of bringing about such large and fast change of the resistance due to its extreme sensitivity to the adsorption of the gas molecules, especially on the tip part of NWs contacting with the graphene.

In conclusion, wafer-scale graphene/Si-NW array heterostructures for molecular sensing were successfully fabricated to show high sensitivity of 37 and 1280% resistance changes within 3.5/0.15 and 12/0.15 s response/recovery times under O_2 and H_2 exposures, respectively, higher than reported before. Graphene played a key role in preventing tips of vertical Si NWs from being bundled, thereby making Si NWs stand on the Si wafer separately from each other under graphene, a critical structural feature for the uniform Schottky-type junction between Si NWs and graphene. The sensor responses were explained based on the surface-transfer doping mechanism. These results strongly suggest that the graphene/Si NW heterostructures can be adopted as various types of Si-NW-based devices such as molecular, photonic, and medical sensors over extended scales.

Methods

Fabrication of vertically-aligned Si NWs. (100)-oriented p type-Si wafers (1–10 Ωcm) were cleaned by using Piranha solution (98% H_2SO_4, 30% H_2O_2, volume ratio = 3 : 1) and then rinsed by deionized (DI) water prior to use. A close-packed monolayer of polystyrene (PS) nano-beads was assembled to have six-fold symmetry on Si wafers by PS lithography method as described below. First, a mixture solution of 4% DI water containing PS nano-beads of 100 nm diameter and ethanol (volume ratio = 1 : 1) was dropped onto top surface of a 5 × 5 cm² SiO_2 (thickness = 300 nm)/Si wafer that was leaned on a petri dish filled with DI water. The dropped mixture solution was then spread on the water surface, resulting in a monolayer of PS nano-beads floating on the water. The nano-bead monolayer was packed closely by dropping a solution of sodium dodecyl sulfate on the water surface, thereby altering the surface tension, and subsequently transferred on a Si wafer and dried (Supplementary Fig. S6a). For the use of the nano-bead monolayer as a mask, RIE was done to reduce the diameter of the nano-beads to ~50 nm, which led to secure the room for making the colloidal particle arrays no longer close-packed (Supplementary Fig. S6b). In the next step, a 15 nm-thick Au thin film was deposited on the nano-bead monolayer by e-beam evaporation, resulting in the formation of Au mesh with hexagonal hole arrays of 100 nm pitch distance and 50 nm hole diameter. By removing the nano-beads in CHCl₃ solution, Au mesh was formed on Si wafer (Supplementary Fig S6c)[40,41]. Si NW arrays were fabricated by metal-assisted chemical etching (MaCE) using Au mesh as a catalyst. The Au mesh/Si wafer was immersed in a mixture solution of HF, H_2O_2, and H_2O (the volume ratio = 1 : 0.5 : 1) for a suitable time, resulting in the formation of uniform Si nanowire (NW) arrays. (Supplementary Fig S6d)[42] The density of Si NWs is in the range of ~10¹⁰/cm², highest ever reported for aligned Si-NW arrays[43]. Finally, the Si NW arrays were dipped in aqua regia (mixture of nitric acid/hydrochloric acid with a volume ratio of 1/3) for a few minutes to remove the Au mesh and particles.

Preparation and characterization of graphene. Graphene layers were grown on 70-μm-thick Cu foils in a halogen-lamp-based chemical-vapour-deposition (CVD) quartz tube furnace at a growth temperature of 1000°C with 10-sccm H_2 and 20-sccm CH_4 flowing at a pressure of 3 Torr during growth[44,45]. The graphene/Cu stack was spin-coated with poly (methyl methacrylate) (PMMA), and the Cu was then etched in a 1 M ammonium persulfate for 10 h. The graphene/PMMA stack is then placed in DI water before transferring to the Si NWs. Detailed transfer process is described elsewhere[46]. Raman spectra were measured by using a 532 nm (~2.33 eV) laser line for excitation to check if the prepared graphene was monolayer (Supplementary Fig. S7). The Raman spectra showed a typical feature of monolayer graphene[41,47]: ~0.45 in the G to 2D band intensity ratio and symmetric 2D band centred at ~2680 cm⁻¹ with a full width at half-maximum (FWHM) of ~35 cm⁻¹.

1. Burda, C., Chen, X., Narayanan, R. & El-Sayed, M. A. Chemistry and properties of nanocrystals of sifferent shapes. *Chem. Rev.* **105**, 1025–1102 (2005).

2. Greene, L. E. *et al.* General route to vertical ZnO nanowire arrays using textured ZnO seeds. *Nano Lett.* **5**, 1231–1236 (2005).
3. Li, Y., Qian, F., Xiang, J. & Lieber, C. M. Nanowire electronic and optoelectronic devices. *Mater. Today* **9**, 18–27 (2006).
4. Law, M., Goldberger, J. & Yang, P. D. Semiconductor nanowires and nanotubes. *Annual Rev. Mater. Res.* **34**, 83–122 (2004).
5. Yang, L. *et al.* Gas sensing of tellurium-modified silicon nanowires to ammonia and propylamine. *Sens. Actuators B* **177**, 260–264 (2013).
6. Taghinejad, H., Taghinejad, M., Abdolahad, M., Saeidi, A. & Mohajerzadeh, S. Fabrication and modeling of high sensitivity humidity sensors based on doped silicon nanowires. *Sens. Actuators B* **176**, 413–419 (2013).
7. Wang, B. & Haick, H. Effect of chain length on the sensing of volatile organic compounds by means of silicon nanowires. *ACS Appl. Mater. Inter.* **5**, 5748–5756 (2013).
8. Chan, C. K. *et al.* High-performance lithium battery anodes using silicon nanowires. *Nat. Nanotechnol.* **3**, 31–35 (2007).
9. Hochbaum, A. I. *et al.* Enhanced thermoelectric performance of rough silicon nanowires. *Nature* **451**, 163–168 (2008).
10. Hochbaum, A. I., Gargas, D., Hwang, Y. J. & Yang, P. D. Single crystalline mesoporous silicon nanowires. *Nano Lett.* **9**, 3550–3554 (2009).
11. Park, M.-H. *et al.* Silicon nanotube battery anodes. *Nano Lett.* **9**, 3844–3847 (2009).
12. Qu, Y. *et al.* Electrically conductive and optically active porous silicon nanowires. *Nano Lett.* **9**, 4539–4543 (2009).
13. Kelzenberg, M. D. *et al.* Enhanced absorption and carrier collection in Si wire arrays for photovoltaic applications. *Nat. Mater.* **9**, 239–244 (2010).
14. Han, H., Kim, J., Shin, H. S., Song, J. Y. & Lee, W. Air-bridged ohmic contact on vertically aligned si nanowire arrays: application to molecule sensors. *Adv. Mater.* **24**, 2284–2288 (2012).
15. Chang, C.-Y. *et al.* Electroluminescence from ZnO nanowire/polymer composite p-n junction. *Appl. Phys. Lett.* **88**, 173503-1–173503-3 (2006).
16. Lai, E., Kim, W. & Yang, P. D. Vertical nanowire array-based light emitting diodes. *Nano Res.* **1**, 123–128 (2008).
17. Xu, S. *et al.* Self-powered nanowire devices. *Nat. Nanotechnol.* **5**, 366–373 (2010).
18. Jeong, H. H. *et al.* Formation of a top electrode on vertical si nanowire devices using graphene as a supporting layer. *Appl. Phys. Exp.* **5**, 105103-1–105102-3 (2012).
19. Novoselov, K. S. *et al.* Electric field effect in atomically thin carbon films. *Science* **306**, 666–669 (2004).
20. Novoselov, K. S. *et al.* Two-dimensional gas of massless Dirac fermions in graphene. *Nature* **438**, 197–200 (2005).
21. Zhang, Y. B., Tan, Y. W., Stormer, H. L. & Kim, P. Experimental observation of the quantum Hall effect and Berry's phase in graphene. *Nature* **438**, 201–204 (2005).
22. Kim, D. H. *et al.* Stretchable and foldable silicon integrated circuits. *Science* **320**, 507–511 (2008).
23. Lee, C., Wei, X. D., Kysar, J. W. & Hone, J. Measurement of the elastic properties and intrinsic strength of monolayer graphene. *Science* **321**, 385–388 (2008).
24. Sekitani, T. *et al.* A rubberlike stretchable active matrix using elastic conductors. *Science* **321**, 1468–1472 (2008).
25. Sze, S. M. & Ng, K. K. The physics of semiconductor devices, 3rd ed. *Wiley Interscience: New York* (2007).
26. Fan, G. F. *et al.* Graphene/silicon nanowire schottky junction for enhanced light harvesting. *ACS Appl. Mater. Inter.* **3**, 721–725 (2011).
27. Xie, C. *et al.* Monolayer graphene film/silicon nanowire array Schottky junction solar cells. *Appl. Phys. Lett.* **99**, 133113-1–133113-3 (2011).
28. Chiesa, M. *et al.* Reversible insulator-to-metal transition in p($^+$)-type mesoporous silicon induced by the adsorption of ammonia. *Angew. Chem. Int. Ed.* **42**, 5032–5035 (2003).
29. Ristein, J. Surface transfer doping of semiconductors. *Science* **313**, 1057–1058 (2006).
30. Yuan, G. D. *et al.* Tunable electrical properties of silicon nanowires via surface-ambient chemistry. *ACS Nano* **4**, 3045–3052 (2010).
31. Fan, Z. Y., Wang, D. W., Chang, P. C., Tseng, W. Y. & Lu, J. G. ZnO nanowire field-effect transistor and oxygen sensing property. *Appl. Phys. Lett.* **85**, 5923–5925 (2004).
32. Wan, Q. *et al.* Fabrication and ethanol sensing characteristics of ZnO nanowire gas sensors. *Appl. Phys. Lett.* **84**, 3654–3656 (2004).
33. Demami, F., Ni, L., Rogel, R., Salaun, A. C. & Pichon, L. Silicon nanowires synthesis for chemical sensor applications. *Proc. Engi.* **5**, 351–354 (2010).
34. In, H. J., Field, C. R. & Pehrsson, P. E. Periodically porous top electrodes on vertical nanowire arrays for highly sensitive gas detection. *Nanotechnol.* **22**, 355501–355505 (2011).
35. Franco, N. *et al.* Structural determination for H_2O adsorption on Si(001)2 × 1 using scanned-energy mode photoelectron diffraction. *Appl. Surf. Sci.* **123–124**, 219–222 (1998).
36. Katırcıoğlu, Ş. & Erkoç, Ş. Adsorption of H_2O on double layer stepped Si(111) surface. *Surf. Sci.* **374**, 208–214 (1997).
37. Zhou, X. T. *et al.* Silicon nanowires as chemical sensors. *Chem. Phys. Lett.* **369**, 220–224 (2003).
38. Chen, Z. H. *et al.* Applications of silicon nanowires functionalized with palladium nanoparticles in hydrogen sensors. *Nanotechnol.* **18**, 345502–345506 (2007).
39. Skucha, K., Fan, Z. Y., Jeon, K., Javey, A. & Boser, B. Palladium/silicon nanowire Schottky barrier-based hydrogen sensors. *Sens. Actuators B* **145**, 232–238 (2010).
40. Huang, Z., Fang, H. & Zhu, J. Fabrication of silicon nanowire arrays with controlled diameter, length, and density. *Adv. Mater.* **19**, 774–748 (2007).
41. Chen, S. *et al.* Synthesis and characterization of large-area graphene and graphite films on commercial cu–ni alloy foils. *Nano Lett.* **11**, 3519–3525 (2011).
42. Kim, J. *et al.* Au/Ag bilayered metal mesh as a si etching catalyst for controlled fabrication of si nanowires. *ACS Nano* **5**, 3222–3229 (2011).
43. Kim, J., Kim, Y. H., Choi, S.-H & Lee, W. Curved silicon nanowires with ribbon-like cross sections by metal-assisted chemical etching. *ACS Nano* **5**, 3222–3229 (2011).
44. Kim, K. S. *et al.* Large-scale pattern growth of graphene films for stretchable transparent electrodes. *Nature* **457**, 706–710 (2009).
45. Bae, S. *et al.* Roll-to-roll production of 30-inch graphene films for transparent electrodes. *Nat. Nanotechnol.* **5**, 574–578 (2010).
46. Jang, C. W. *et al.* Rapid-thermal-annealing surface treatment for restoring the intrinsic properties of graphene field-effect transistors. *Nanotechnol.* **24**, 405301 (2013).
47. Wang, Y. Y. *et al.* Raman studies of monolayer graphene: the substrate effect. *J. Phys. Chem.* **112**, 10637–10640 (2008).

Acknowledgments

Author contributions

J.H.K. deposited graphene sheets by CVD. S.D.O. prepared patterning masks for the fabrication of well-aligned Si NWs. D.H.S. did structural characterization of graphene. J.K. fabricated Si NWs and molecular sensors, characterized performances of molecular sensors, and wrote the paper. S.K. measured the *I-V* characteristics. S.-H.C. initiated, supervised the work, and wrote the paper. All authors discussed the results and commented on the manuscript.

Additional information

Supplementary information accompanies this paper at http://www.nature.com/scientificreports

Competing financial interests: Yes, there is potential Competing Interest. S.-H.C., S.K., J.K., and D.H.S. have a Korea patent pending (10-2013-0084226) on the graphene/Si-NW molecular sensor production technology, reported in this paper.

How to cite this article: Kim, J. *et al.* Graphene/Si-nanowire heterostructure molecular sensors. *Sci. Rep.* **4**, 5384; DOI:10.1038/srep05384 (2014).